Mobile Domain Walls as a Bridge between Nanoscale Conductivity and Macroscopic Electromechanical Response

Tadej Rojac, Hana Ursic, Andreja Bencan, Barbara Malic, and Dragan Damjanovic*

The interfaces in complex oxides present unique properties exploitable in nanoscale devices. Recent studies on ferroelectric $BiFeO_3$, $BaTiO_3$, and $Pb(Zr,Ti)O_3$ have revealed an unusually high electric conductivity of the domain walls (DWs), adding another degree of freedom for controlling the local properties of these materials. While most of the investigations are focused on thin films for nanoscale applications, many practical devices, including piezoelectric sensors, actuators, and transducers, rely on the macroscopic properties of bulk polycrystalline materials where the average effect of local properties should be small. It is shown that in polycrystalline $BiFeO_3$ the local domain-wall conductivity interferes with the dynamics of the DWs within the grains, resulting in an unexpectedly large effect on the macroscopic piezoelectric response. The results thus bridge the local conductivity and the macroscopic piezoelectricity via domain-wall dynamics, revealing that the domain-wall conductivity must be considered when interpreting and controlling macroscopic electromechanical properties.

1. Introduction

The interfaces in complex oxides can display properties that are entirely different to those of the surrounding matrix material(s). Due to the boundary conditions to which these planar defects are exposed, they often exhibit unexpected and unique behaviors. Examples include the superconductivity at an artificially created interface between two insulating perovskites[1] and the large weak-field magnetoresistive effect across a grain boundary.[2]

With numerous possibilities for nanoscale applications, of particular interest are the interfaces in single- and multiphase ferroic (ferroelectric, ferroelastic, and (anti)ferromagnetic) oxide systems.[3–12] A special type of interface in ferroic materials is the domain wall (DW). DWs are naturally formed boundaries that separate distinct domains with a different orientation of the order parameter (spontaneous polarization, strain, or magnetization). Recent theoretical and experimental studies,[3–6] first performed by Seidel et al.[3] on thin films of $BiFeO_3$, and later by other authors on $Pb(Zr,Ti)O_3$ (PZT) thin films,[8,9] and single crystals of $LiNbO_3$[10] and $BaTiO_3$,[12] revealed unusually high electric conductivity of the ferroelectric and ferroelastic DWs. This opens up a whole new and emerging field of domain-wall nanoelectronics, whereby local conductivity at the DWs may be exploited in nanodevices.[3,13,14]

Most of the current studies on conductive DWs are based on nanoscale effects. It is expected that, in the absence of percolation, these local properties should average out to a small or zero effect on a macroscopic scale. Exceptions include single crystals[12] and thin films,[3] where the DWs can extend continuously between two surfaces of the sample. For this reason, the potential role of nanoscale conductivity, particularly of the DWs, on macroscopic electromechanical response of polycrystalline ferroelectrics with randomly oriented grains has not been so far given sufficient attention. These materials are employed in a vast majority of piezoelectric devices, so that the question has important technological implications. Even if the local conductivity within the DWs does average macroscopically to a small value, the dynamics of DWs may still be strongly affected by their conductivity. Such an effect would be important because domain-wall motion has a dominant influence on the dielectric and piezoelectric properties of ferroelectric materials, contributing up to 70% of the total macroscopic response.[15–17] It is therefore possible to envision that the local conductivity at the DWs may interfere with the domain-wall dynamics and, thus, indirectly affect the macroscopic electromechanical response of polycrystalline ferroelectrics, even if the direct average effect of the local conductivity on the properties is small. Such coupling between the local conductivity at the DWs and their dynamics would open up a new method for controlling the macroscopic electromechanical properties of ferroelectrics, similar to the way a small concentration (<1%) of aliovalent dopants can control domain-wall displacement, leading to the technologically important "soft" and "hard" ferroelectrics.[18] In the present case, the parameter that controls the domain-wall motion would be the conductivity of the DWs. This effect is fundamentally different from the recent demonstration that charged and conducting DWs in single crystals of $BaTiO_3$ lead to a large enhancement of the macroscopic dielectric and piezoelectric properties.[19] That mechanism requires

Prof. T. Rojac, Dr. H. Ursic, Prof. A. Bencan, Prof. B. Malic
Electronic Ceramics Department
Jozef Stefan Institute
Jamova cesta 39, 1000 Ljubljana, Slovenia
E-mail: tadej.rojac@ijs.si
Prof. D. Damjanovic
Ceramics Laboratory
Swiss Federal Institute of Technology – EPFL
Station 12, STI IMX
1015 Lausanne, Switzerland

DOI: 10.1002/adfm.201402963

a special type of engineered DWs, which are obtained using a specific poling procedure, so-called "frustrated poling," and in which case the charges on static DWs destabilize the material between the walls through a depolarizing electric field.

In this paper we provide evidence for the existence of spontaneously formed, conductive DWs in polycrystalline $BiFeO_3$. We show that these conducting interfaces persist in poled material and move significantly under subswitching driving fields, contributing strongly and in an unusual way to the macroscopic piezoelectric response. We reveal several emerging features as a result of the dynamics of conducting DWs, including the low-frequency nonlinear piezoelectric Maxwell–Wagner (M–W) mechanism and the associated large enhancement of the piezoelectricity, which have not been demonstrated so far in ferroelectrics. The results suggest a new route for the control of macroscopic electromechanical properties of polycrystalline ferroelectrics by coupling the domain-wall dynamics with the conductivity of the DWs. We thus expect that this study may have broader consequences on the engineering of the properties of ferroelectric ceramics and single crystals.

2. Results and Discussion

2.1. Macroscopic Piezoelectric Response

We begin by illustrating the fundamental difference between the macroscopic piezoelectric response of $BiFeO_3$ and conventional, technologically most widely used ferroelectric ceramics, i.e., morphotropic donor-doped PZT. As will be shown in this section, the piezoelectric behavior of $BiFeO_3$ is distinctly different from that of PZT. It will be demonstrated that the mechanisms of domain-wall motion in "disordered" ferroelectrics, which are exemplified by the donor-doped PZT, cannot be applied to the case of $BiFeO_3$. The macroscopic response is presented in terms of the longitudinal piezoelectric coefficient, d_{33}, and the tangent of the piezoelectric phase angle, tanδ, as a function of driving electric-field frequency, f (**Figure 1**).

In general, two types of frequency dependences of the piezoelectric coefficient d were observed in morphotropic PZT: (i) frequency independent, which is found in acceptor-doped "hard" PZT and which, according to permittivity data, persists up to the GHz range,[20] and (ii) logarithmic dependence $d \approx \log(1/f)$, observed in donor-doped "soft" PZT. The latter case is shown in Figure 1a. In general, this linear-logarithmic behavior appears in "disordered" ferroelectric systems and is interpreted in terms of the field-induced motion of DWs in a medium with random pinning centers.[21,22]

In striking contrast to PZT, $BiFeO_3$ exhibits a frequency dispersion that is characterized by an abrupt increase in d_{33} and tanδ at low frequencies (<4 Hz, Figure 1b). Obviously, such behavior cannot be understood by considering the well-accepted mechanisms for "soft" PZT and other "disordered" ferroelectrics. In addition to the large relative increase of d_{33} from 100 to 0.2 Hz (76% for $BiFeO_3$ and 18% for PZT), the piezoelectric

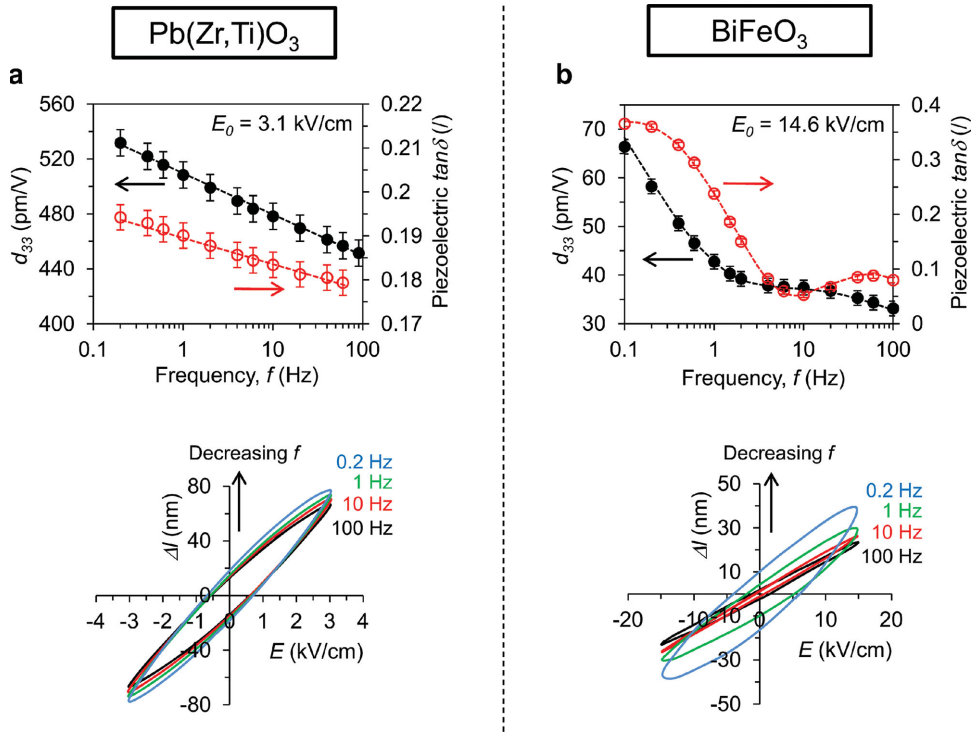

Figure 1. Comparison of converse piezoelectric response of PZT and $BiFeO_3$ ceramics. Piezoelectric d_{33} coefficient and tanδ as a function of frequency of the driving electric field for a) Nb-doped morphotropic PZT and b) $BiFeO_3$ ceramics. The broken lines are drawn as a guide for the eye. The driving-field amplitudes (E_0) are noted on the graphs. The two materials were driven under a comparable field relative to the coercive ($E_0/E_{coercive} \approx 20\%$ for both PZT and $BiFeO_3$). The corresponding subswitching Δl–E hysteresis loops of the two materials, measured at 100, 10, 1, and 0.2 Hz, are also shown. Note the very different piezoelectric behavior: a log(1/f) dispersion of d_{33} and tanδ in PZT (panel a)) versus a low-frequency (<4 Hz) M–W-like d_{33} dispersion accompanied by a large hysteresis characteristic for the $BiFeO_3$ (panel (b)).

tanδ of $BiFeO_3$ is significantly more affected by the frequency than that of PZT (compare tan δ in Figure 1a,b). The piezoelectric response of $BiFeO_3$ is weakly hysteretic at high frequencies, as seen from the mechanical-displacement–electric-field (Δl–E) hysteresis loops at 100 and 10 Hz in Figure 1b and becomes strongly hysteretic once the driving frequency is reduced (see loops at 1 and 0.2 Hz in Figure 1b). In contrast, PZT exhibits a strong hysteretic response across the whole frequency range, with minor changes in the hysteresis area as the frequency is varied (see PZT loops in Figure 1a).

In the next step we investigate the origin of the piezoelectric frequency dispersion of $BiFeO_3$ and show that it is related to nonlinear, irreversible domain-wall displacements at low driving frequencies. This can be demonstrated by measuring the dependence of d_{33} on the driving-field amplitude (i.e., piezoelectric nonlinearity), and by analyzing the Δl–E hysteresis loops. Typically, in ferroelectric materials the nonlinearity and the hysteresis of the piezoelectric response at subswitching fields can be associated with the irreversible motion of non-180° DWs.[21,23–25] For our present purpose, we conducted piezoelectric measurements on $BiFeO_3$ as described previously for Figure 1b, but this time introducing the electric-field amplitude, E_0, as a second external parameter (**Figure 2**). The functions $d_{33}(f, E_0)$ (Figure 2a) and tan $\delta(f, E_0)$ (Figure 2b) can be subdivided into two distinct frequency regions: first, a high-frequency region where d_{33} and tanδ are quasi-independent of E_0 and a second, low-frequency region where both are dependent on E_0. The data thus clearly show that the piezoelectric nonlinearity and the associated hysteresis appear only when the material is driven at low frequencies. The low-frequency dispersion and nonlinearity are correlated, suggesting that both have origin in the irreversible non-180° domain-wall displacements.

In addition to the nonlinear contribution, we analyze the linear (field-independent) contribution to the piezoelectricity by plotting d_{33} and tanδ extrapolated at zero field ($E_0 = 0$) for each frequency (open circles in Figure 2a,b). In general, the linear component of the piezoelectric coefficient includes contributions from the intrinsic (lattice) piezoelectric effect, the reversible domain-wall motion[21,23,25] and other linear mechanisms, such as the M–W effect,[26] which couples piezoelectricity with the electrical conductivity. The linear contribution of the piezoelectric response of $BiFeO_3$ is characterized by a nonmonotonic frequency dispersion of d_{33} and tan δ, together with a negative piezoelectric phase angle in the region ≈2–10 Hz (see arrow in Figure 2b).

There are two remarkable features of the piezoelectric response of $BiFeO_3$. The first is the low-frequency piezoelectric nonlinearity (Figure 2a) and the corresponding nonlinear hysteresis (Figure 2b) accompanied by the strong frequency dispersion. We note that this unusual nonlinear dispersion is qualitatively common for a number of $BiFeO_3$ samples that we prepared with different processing parameters. In addition, the dielectric permittivity of $BiFeO_3$ shows the same low-frequency nonlinearity (see Supporting Information Figure S1). As already stated above, the piezoelectric nonlinearity accompanied by the hysteresis implies a contribution from the irreversible motion of non-180° DWs, whose mechanism in $BiFeO_3$ is distinctly different from that in "disordered" ferroelectrics,

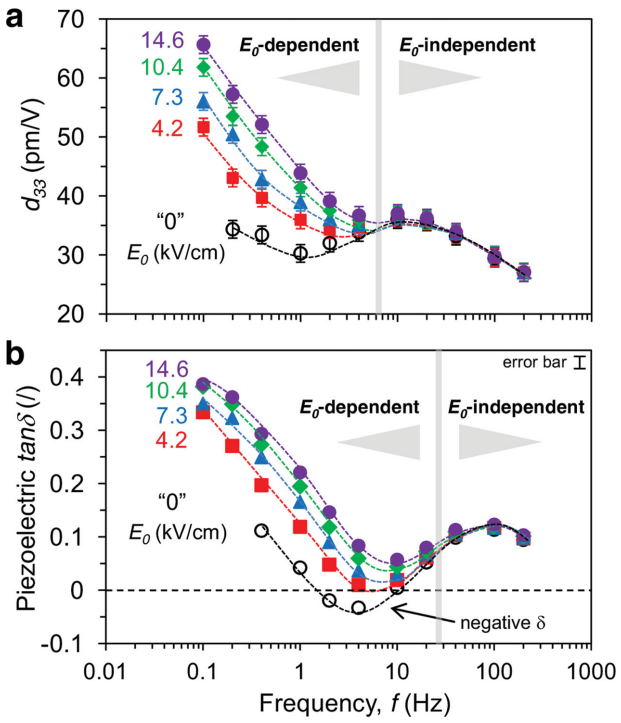

Figure 2. Frequency dispersion and field dependence of the converse piezoelectric response of $BiFeO_3$ ceramics. a) Piezoelectric d_{33} coefficient and b) tanδ as a function of frequency (f) and amplitude (E_0) of the driving electric field. The linear ("E_0-independent") dispersion regime in the high-frequency range and the nonlinear ("E_0-dependent") dispersion regime in the low-frequency range are indicated by a line and arrows in respective graphs. The $d_{33}(f)$ and tan$\delta(f)$ curves denoted as "$E_0 = 0$" (open circles in panels (a,b)) were obtained by extrapolating the $d_{33}(f, E_0)$ and tan$\delta(f, E_0)$ relationships to $E_0 = 0$ for each frequency and represent the linear (field-independent) contribution to the piezoelectric response. This linear contribution to d_{33} exhibits a negative piezoelectric phase angle as indicated by an arrow in panel (b).

which are characterized by the log(1/f) nonlinearity (compare panels a and b in Figure 1). In addition to the irreversible motion, it is reasonable to assume that a subset of the DWs also moves reversibly, possibly by bending, contributing to the linear component of the total piezoelectric response (open circles in Figure 2).

To show quantitatively that the contribution from the irreversible domain-wall displacements to the piezoelectricity in $BiFeO_3$ at low frequencies is indeed as large as in "soft" ferroelectric materials, we compare the converse piezoelectric response of $BiFeO_3$ with that of the "soft" morphotropic PZT. A way to do this quantitatively is by calculating the fraction of the total d_{33} that is due to the irreversible domain-wall displacements (X_{IR}) at selected maximum electric-field amplitude (E_0^{max}):

$$X_{IR} = \frac{d_{33}(E_0^{max}) - d_{33}(0)}{d_{33}(E_0^{max})} \quad (1)$$

where $d_{33}(0)$ is the coefficient extrapolated at zero field ($E_0 = 0$). In case of $BiFeO_3$ at 0.2 Hz and $E_0^{max} = 14.6$ kV cm^{-1} (Figure 2a),

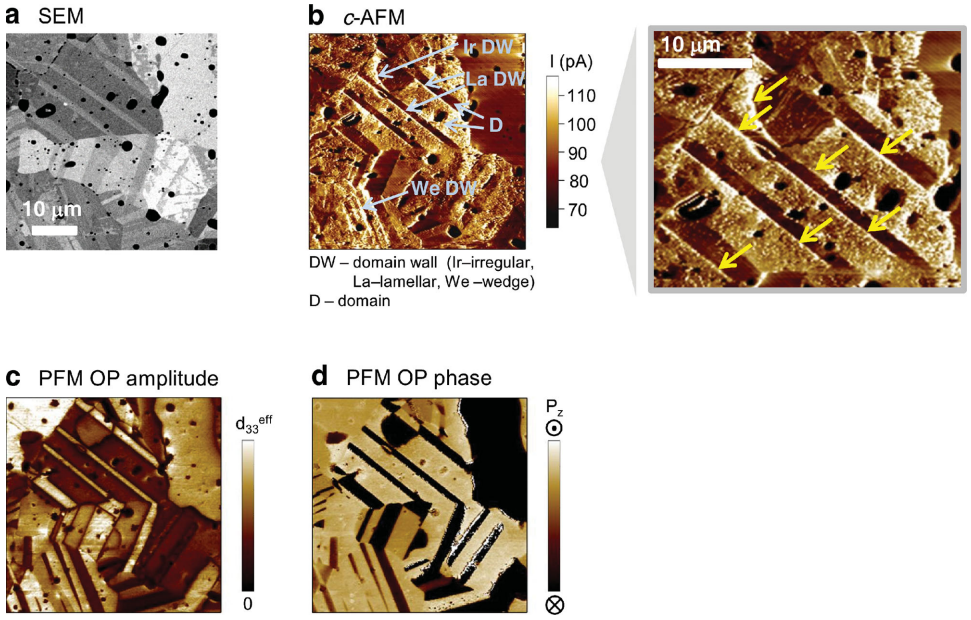

Figure 3. Domain structure and local electrical conductivity of $BiFeO_3$ ceramics. a) BE SEM micrograph, b) *c*-AFM image, and OP PFM c) amplitude and d) phase images of same selected area in as-sintered $BiFeO_3$ ceramics. The *c*-AFM image was acquired by applying +33 V of DC voltage to the tip. Regions with enhanced local conductivity, including whole areas inside the domains (D) and DWs of different morphological type, are highlighted on the *c*-AFM image in panel (b). The inset of panel (b) shows an enlarged view of the conductive DWs (see arrows). The dark, irregularly shaped and spherical-like regions in panel (a) are pores.

this fraction accounts for 40% of the total d_{33}, reaching levels comparable to those of "soft" morphotropic PZTs.[23,25]

The second interesting feature of our results is the negative piezoelectric phase angle (Figure 2b) and the corresponding hysteresis loop with a clockwise sense of rotation, which were also confirmed by direct piezoelectric measurements of $BiFeO_3$.[27] Both are signatures of the M–W piezoelectric mechanism, which is the piezoelectric analogue of the more common dielectric M–W effect[28] and has been observed in heterogeneous and composite piezoelectric materials.[26,29] The piezoelectric M–W mechanism arises due to the coupling of the piezoelectric and dielectric properties, whereby the electrical conductivity affects the piezoelectric response indirectly through the presence of local regions in the ceramics that provide conductive paths and modify the piezoelectrically induced charges at the interfaces within the sample.[26,30,31] As will be shown in the next section, these local conductive regions may be, for example, grain boundaries, interfaces with secondary phases or DWs. Theoretical models show that the M–W effect may lead to a negative piezoelectric phase angle, which was confirmed experimentally,[26,29] and to a huge enhancement of the piezoelectricity in heterogeneous piezoelectric materials at low frequencies[32] (for additional explanations see Supporting Information S2).

While the piezoelectric nonlinearity links the piezoelectric response to the irreversible domain-wall motion, the M–W mechanism suggests locally conductive regions in the ceramics (or variations in the conductivity between different regions on a local scale). Observing both phenomena in the same material is consistent with the presence of conductive DWs. Next we present evidence for the conductive DWs in bulk polycrystalline $BiFeO_3$.

2.2. Conductive DWs in Bulk $BiFeO_3$

The domains and DWs in $BiFeO_3$ were mapped using a combination of backscattered-electron (BE) scanning electron microscopy (SEM) imaging (**Figure 3**a) and piezoresponse-force microscopy (PFM) imaging, where out-of-plane (OP) amplitude and phase signals were analyzed (Figure 3c,d). Note that the microscopy data presented in this section (the only exception is Figure 7c,d) and in Supporting Information Figures S3–S6 refer to "coarse-grained" (CG) $BiFeO_3$ samples, while the macroscopic measurements were performed on "fine-grained" (FG) $BiFeO_3$. The preparation procedure of "FG" and "CG" samples is described in the Experimental Section. The "CG" $BiFeO_3$ was selected for the domain analysis as in these samples it was easier to identify the DWs and their conductivity because of the large grains. We emphasize that the macroscopic piezoelectric behavior of these two kinds of samples is qualitatively the same and mutually consistent. Due to this similarity, the macroscopic piezoelectric response of "CG" $BiFeO_3$ is not reported.

Morphologically, three types of domains were identified in $BiFeO_3$ ceramics, i.e., lamellar-like, wedge-like, and irregularly shaped (marked in Figure 3b as La DW, We DW, and Ir DW, respectively). Additional PFM images of these domains are reported in the Supporting Information Figure S3. The rather large domains (≈1–10 μm, Figure 3), also observed by other authors,[33] are consistent with the large grains of this sample ($\langle d_{grain} \rangle = 16.0 \pm 8.5$ μm).

The local electric current mapping (Figure 3b), carried out with conductive atomic-force microscopy (*c*-AFM), and combined with SEM (Figure 3a) and PFM imaging (Figure 3c,d) of the same sample area, revealed two features: (i) variations in the current signal between adjacent domains (see D in

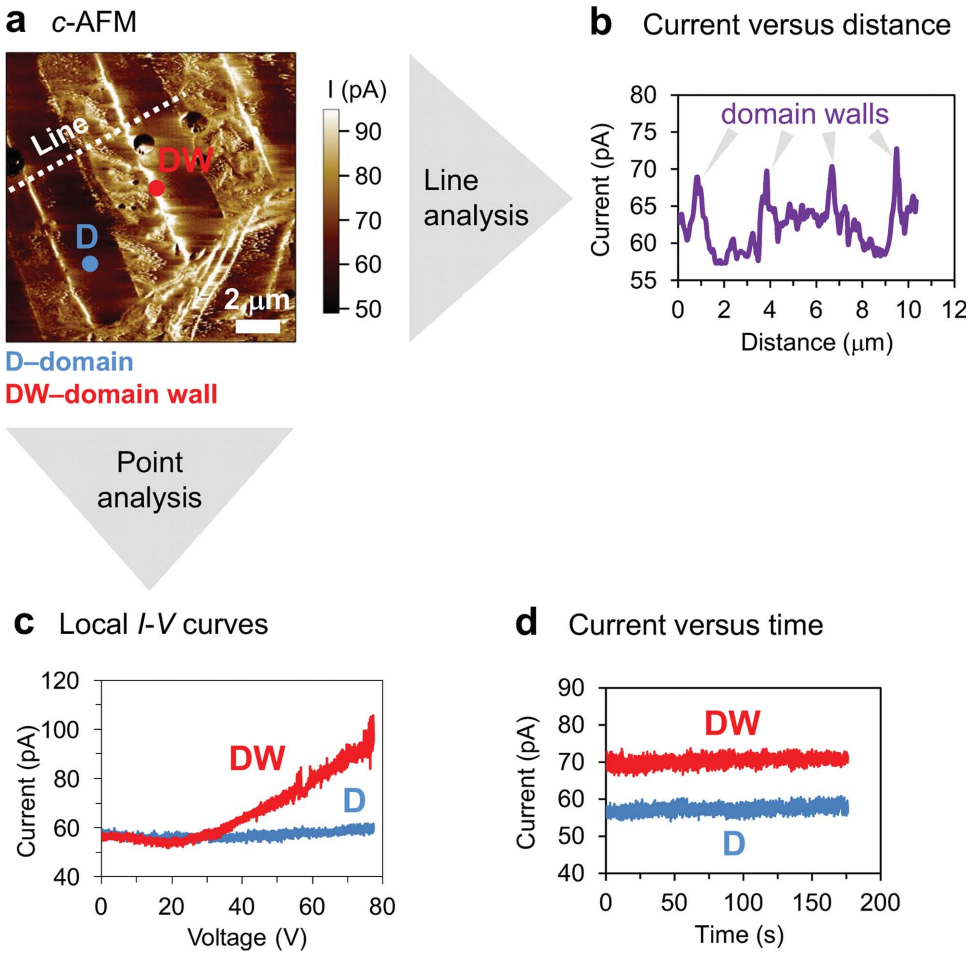

Figure 4. Conductive DWs in as-sintered $BiFeO_3$ ceramics. a) *c*-AFM image of a region with lamellar-like domains, b) current profile across DWs (see line in panel (a)), c) local *I–V* curves obtained by positioning the tip in the domain area (point D, panel (a)) and at the DW (point DW, panel (a)), and d) time dependence of current, measured by positioning the tip at the domain or DW. The current signal, shown in panels (a,b,d), was acquired at +33 V of DC bias applied to the tip. By analyzing the local *I–V* response of several DWs, the onset of the current increase, as seen in panel (c) (DW), was found typically at voltages between ≈10 and ≈30 V. The time-dependent currents, shown in panel (d), were measured close to, but not exactly at positions D and DW as noted in panel (a).

Figure 3b) and (ii) an enhanced current signal at the DWs (see Ir DW, La DW, and We DW in Figure 3b and Supporting Information Figure S3 for additional *c*-AFM images).

The difference in the conductivity between some domains is likely due to the different orientation of the spontaneous polarization, which may affect the height of the Schottky barrier at the sample/AFM-tip interface and, thus, the current flow during *c*-AFM imaging, as discussed recently for $BiFeO_3$ thin films by Farokhipoor and Noheda.[34] The interaction between spontaneous polarization and Schottky barriers is well known to occur in ferroelectric ceramics, as reported for $BaTiO_3$.[35]

To confirm the existence of spontaneously formed conductive DWs in as-sintered $BiFeO_3$ samples, we performed a set of experiments with the AFM, the results of which are summarized in **Figure 4**.

The current profile, as we scanned with the AFM tip across different domains (see dotted line in Figure 4a), revealed distinct peaks in the measured current at positions that correspond to the DWs (Figure 4b).

The local current–voltage (*I–V*) response was measured by positioning the AFM tip either on a domain or a DW (see points D and DW in Figure 4a). At each of these positions, the voltage was increased from 0 to ≈80 V with a linear ramp of 1 V s^{-1} and the current through the tip was monitored (Figure 4c). In contrast to the rather high resistance of the domain's interior, characterized by little dependence of the current on voltage (Figure 4c, D), the current measured at the DW exhibited a quasi-linear voltage dependence with an onset at ≈30 V (Figure 4c, DW). The voltage-activated conduction at the wall is consistent with the behavior of $BiFeO_3$ thin films[3,4] and confirms the conductive character of the walls in bulk $BiFeO_3$. Note that the *I–V* curves reveal a background current of ≈60 pA at the proximity of zero voltage (see Experimental Section for details about its origin). The presence of this offset current during measurements, however, does not affect the conclusion on the higher conductivity of the DWs relative to the domains' interior. We also note that the conductive DWs were identified by scanning with the AFM tip biased with a negative DC voltage (Supporting Information Figure S4).

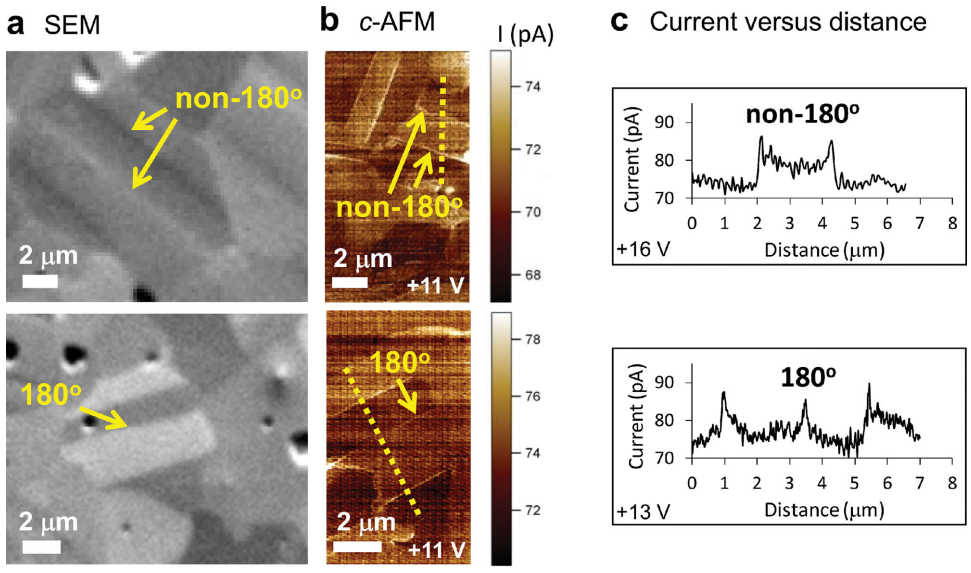

Figure 5. Conductive 180° and non-180° (71° and/or 109°) DWs in $BiFeO_3$ ceramics. a) BE SEM micrographs and b) *c*-AFM images of the same region with DWs. c) Current profiles across DWs (see dotted lines in panel b)). DC biases used for *c*-AFM imaging and current profiles are indicated. The different types of DWs were identified by EBSD analysis.

To further explore the time-stability of the local current signal, we measured the current by exposing the domain or the DW to a constant DC bias of +33 V for ≈3 min. In comparison to the current signal within the domain (Figure 4d, D), a persistently higher current was measured at the wall during prolonged DC voltage exposure (Figure 4d, DW) with no change in the domain configuration. This confirms the true steady conduction behavior of the walls. Finally, the observed enhanced current signal at the DWs was found to not correlate with the sample topography (Supporting Information Figure S5).

Additional *c*-AFM analyses on different regions, similar to that shown in Figure 3b, confirmed that DWs of all identified domain morphologies, i.e., lamellar-like, wedge-like, and irregular, were accompanied by an enhanced current signal. Considering this observation and the fact that, over numerous AFM/PFM experiments, we could not identify distinct regions with systematically lower or no current signal at the DWs, we reasonably assume that both 180° and non-180° (71° and 109°) DWs may be conductive in bulk $BiFeO_3$, which is consistent with the reports on $BiFeO_3$ thin films.[4] We confirmed the conductivity of 180° and non-180° (71° and/or 109°) DWs by analyzing the $BiFeO_3$ samples using a combination of electron-backscattered diffraction (EBSD) and *c*-AFM measurements, the results of which are shown in **Figure 5**.

In the search of the link between conducting DWs and macroscopic piezoelectricity, it is essential to demonstrate the conductivity of the walls in poled samples because the poling is necessary to induce a macroscopic piezoelectric response in polycrystalline samples. The conducting DWs in poled samples are revealed in two different ways: (i) by probing local currents with *c*-AFM in ex situ macroscopically poled samples (see Supporting Information Figure S6) and (ii) by switching domains in situ with the AFM tip (**Figure 6**). Even though the field distribution and thus the switching process in the samples during the two poling procedures are different, the experiments independently confirmed the existence of conductive DWs after both poling processes.

The results of the AFM in situ switching experiments are shown in Figure 6. A selected area of the sample (Figure 6a,b) was first poled by scanning the biased tip across the area. The resulting switching process occurred inhomogeneously throughout the biased area, so that certain regions were more affected than others (Figure 6c,d). For example, in the region denoted as r1 (see Figure 6c and compare with Figure 6a) new DWs were nucleated, in region r2 (Figure 6c) the walls grew from preexisting ones (see also same r2 region in Figure 6a), whereas other regions were morphologically less affected by the poling (see r3 in Figure 6c and compare with Figure 6a). After this poling procedure, the current map clearly revealed that all these types of DWs are conductive (Figure 6e, circles). From these results, those on the macroscopically poled samples (Supporting Information Figure S6) and the results on the as-sintered samples (Figure 3, 4, and 5), we can conclude that the poling procedure, which is necessary for macroscopic piezoelectricity, does not qualitatively alter the conductive character of the DWs. We can therefore also assume that the conductive nature of the DWs in $BiFeO_3$ is not affected by the field used to measure the macroscopic piezoelectric response.

It is worth mentioning that the AFM in situ switching experiments did not reveal the behavior described by Stolichnov et al.[36] in which case the displacement of DWs in $BiFeO_3$ thin film left conductive traces at the original domain-wall positions. In our case, we observed that the conductive paths after the switching process do coincide with the new (switched) positions of the DWs (compare panels c–e in Figure 6). In general, defects and charge carriers in thin films and ceramics may be different and it is possible that, unlike in thin films, in $BiFeO_3$ ceramics the defects that are responsible for the conductivity of the DWs are mobile and thus move along with the walls when field is applied.

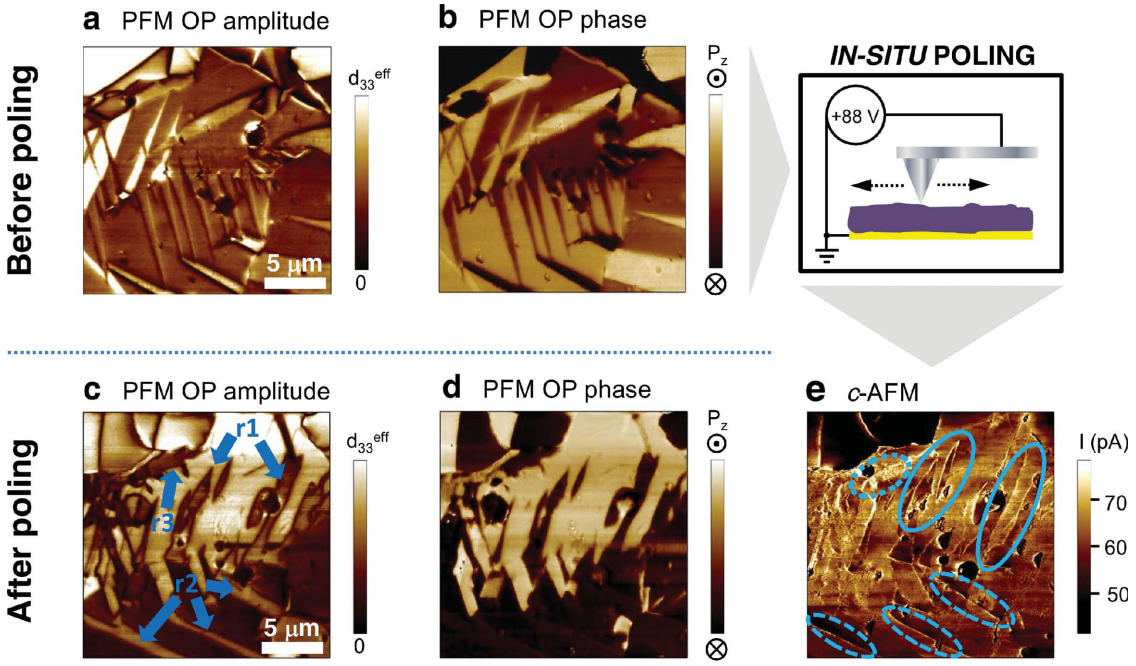

Figure 6. Conductive DWs in $BiFeO_3$ ceramics after in situ poling with the AFM tip. OP PFM amplitude and phase images of the same region a,b) before and c,d) after in situ poling with the AFM tip; e) *c*-AFM image after poling. As shown in the schematics, the region was poled by scanning with the AFM tip across the area with +88 V of DC bias. The *c*-AFM image (panel (e)) was acquired after this poling procedure with the tip biased at +33 V. This lower bias was used to avoid further domain switching. Note from panel e) that newly nucleated DWs (full circles), the ones that grew during poling from preexisting walls (broken-line circles) and the ones that were less affected by the tip bias (dotted circles) all show conductive character. These same regions are marked respectively as r1, r2, and r3 on PFM image in panel (c).

To compare with $BiFeO_3$, we carried out AFM/PFM analyses on the as-sintered and poled PZT bulk samples. Among the undoped, "hard" and "soft" PZT of different compositions (see Experimental Section), we were not able to identify conductive DWs, at least not to such an extent and under the same experimental condition as in the case of $BiFeO_3$ (not shown). Therefore, the distinct behavior of the macroscopic piezoelectric response of $BiFeO_3$, as compared to that of PZT (see Figure 1), in particular the low-frequency nonlinearity (Figure 2), is likely associated with the presence and motion of conductive DWs in the ferrite. Considering that the DWs are, at the same time, conducting and mobile, the mechanism by which the irreversible motion of conducting DWs may affect the macroscopic piezoelectric response of $BiFeO_3$ is the "nonlinear M–W effect".

While the presence of conductive DWs explains the dispersive nonlinear behavior and the negative piezoelectric phase angle, we should consider other regions conductive at the local level, which may not be mobile under the fields used here, but which may contribute to the macroscopic properties through the *linear* M–W mechanism. In the direct piezoelectric effect (an analogous principle is valid for the converse piezoelectricity),[31] the M–W mechanism arises whenever two phases with different piezoelectric properties and conductivities meet, in which case the uncompensated piezoelectric charges created at the interface between these two phases due to the different piezoelectric coefficients are dissipated by the conduction through the materials.[26,30] In the present case, one of the two phases may be the $BiFeO_3$ matrix, while the other, which can be nonpiezoelectric, may be secondary phases, which are frequently reported in the literature for $BiFeO_3$[37] and were also identified in our ceramics (see Experimental Section). In another scenario it is possible to envision uncompensated piezoelectric charges at the interface between two differently oriented $BiFeO_3$ grains decaying with time through the conducting grain boundaries, and thus affecting the macroscopic piezoelectricity. To investigate for these possibilities, we looked for locally conducting features other than DWs.

Figure 7 shows SEM and *c*-AFM images of the selected regions in $BiFeO_3$ ceramics where we identified two features: (i) conductive grain boundaries at triple-grain junction (Figure 7b) and (ii) the absence of a significant current signal in a region that corresponds to Bi-rich and Fe-rich secondary phases (Figure 7d). Note also the increased current appearing at the interface between the $BiFeO_3$ and the nonperovskite phases (see right part of Figure 7d). The variation in conductivity between the matrix phase and these local regions could, in principle, lead to the *linear* M–W piezoelectric effect and to the macroscopically measured negative piezoelectric phase angle. However, the strong low-frequency piezoelectric nonlinearity, which accounts for as much as 40% of the total piezoelectric response at low frequencies, as shown by the calculation described earlier (Equation (1)), and the nonlinear hysteresis (Figure 2), can only be explained by the irreversible motion of the conducting non-180° DWs. The reason is that for the fields used here, neither the grain boundaries nor the interfaces with secondary phases are expected to exhibit a dynamic character.

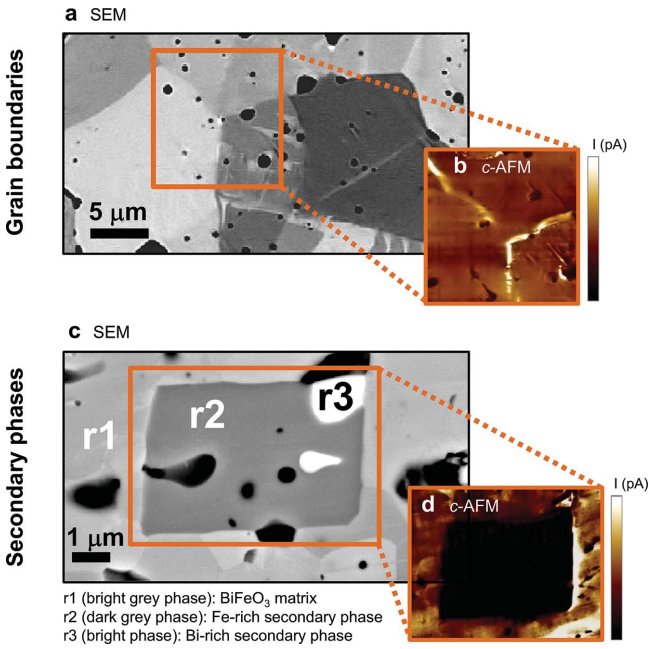

Figure 7. Local electric current at grain boundaries and in secondary (non-perovskite) phases. a,c) BE SEM images of local regions in $BiFeO_3$ ceramics and b,d) *c*-AFM images of same areas, showing b) conductive grain boundaries and d) the absence of a significant current signal in the Bi-rich and Fe-rich secondary phases. Current images under b) and d) were acquired by scanning the area with +88 and +10 V of DC bias, respectively. The secondary phases were identified by means of EDXS and were analyzed in "FG" $BiFeO_3$ sample (see Experimental Section). The black, rounded-like and irregular features in the SEM images are pores.

These other conducting features may thus still contribute to the piezoelectric dispersion, but only to its linear part through the *linear* M–W mechanism.

3. Conclusions

By combining macroscopic piezoelectric measurements and local probing of the electrical conductivity in polycrystalline $BiFeO_3$, we established a link that relates the local conductivity of the individual DWs with their collective and dynamic contribution to the macroscopic properties. Our analysis demonstrates that the conductive DWs, which were previously discussed only in thin films, are a general property of bulk $BiFeO_3$ and exist in both as-sintered and poled ceramics. We have shown that these DWs are mobile under subswitching electric fields, leading to a large enhancement of the macroscopic electromechanical response, large piezoelectric hysteresis and a strong frequency dispersion, particularly when the material is stimulated by intensive and low-frequency fields. Such driving conditions proved to be the most favorable for an irreversible displacement of DWs with a conductive character, probably because depinning of DWs from charged defects is easier if conductivity is available at the walls.[38] In contrast, at higher frequencies and low fields, where little or no charge transport occurs through the walls, the conducting DWs are pinned and only move reversibly, probably by bending. We showed that this unique behavior of $BiFeO_3$ is distinctly different from that

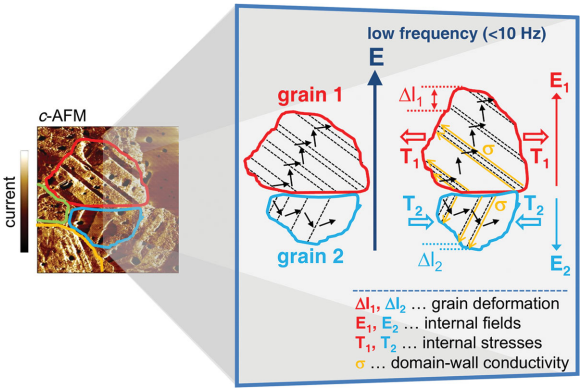

Figure 8. Schematics of nonlinear M–W piezoelectric effect arising from conducting DWs. The case considers a heterogeneous system consisting of two or more phases, which can be individual grains in a polycrystalline ceramics. When an external electric field *E* (as shown in the schematic) or stress field *T* is applied to such a material, the different piezoelectric, dielectric, and elastic responses of each individual phase induce internal electric E_{int} and stress fields T_{int}. These internal fields act upon the material in addition to the external *E* or *T* fields (see schematic) and modify the total response of the system.[30–32] A specific situation arises inside the material when a phase (or grain) exhibits appreciable electric conductivity, which modifies the internal fields and, thus, the total response of the heterogeneous system. This is the origin of the M–W dielectric and electromechanical relaxations, which are usually considered as linear phenomena, i.e., they do not depend on the magnitude of the external *E* or *T* field. In ferroelectric materials, if DWs move irreversibly at low or moderate fields, the response of each grain becomes a nonlinear function of the field magnitude and can be described by Rayleigh relations.[21] If the walls are also conducting, as illustrated in the schematic, the combination of the conductivity through the walls and the nonlinearity induced by their irreversible motion leads to nonlinear M–W relaxation, as observed here in $BiFeO_3$. The effect is dominant at low driving frequencies where the DWs are rather mobile because their conductivity helps in the depinning from charged defects.[38]

of morphotropic PZT and other "disordered" ferroelectrics, in which the DWs can move irreversibly at higher frequencies, leading to a logarithmic dispersion of the piezoelectric response.

As opposed to the usually considered piezoelectric M–W effect, which refers to a *linear* process,[26,30–32] the results of this work demonstrate a *nonlinear* M–W piezoelectric effect as a consequence of the dynamics of conducting DWs. A simplified schematic of this mechanism is shown in **Figure 8**. The unique coupling between the local conductivity and the macroscopic piezoelectric nonlinearity is achieved through the DWs as they provide, at the same time, local conductive paths through the grains, which is required for the M–W effect, and macroscopic nonlinearity through their irreversible motion.

Though we confirmed that the conductive DWs may account for a great part of the piezoelectric response of $BiFeO_3$ through the nonlinear M–W effect, other locally conductive regions identified in $BiFeO_3$, such as the grain boundaries, and variation in the conductivity between the secondary phases and the matrix $BiFeO_3$ phase, may influence the field-independent (linear) piezoelectric response through the *linear* M–W effect.

The presented results offer a new degree of freedom in the control of the electromechanical properties of ferroelectric ceramics through the conductivity of the DWs and may have

broader consequences in the emerging field of high-temperature piezoelectrics based on $BiFeO_3$.[39–41] For example, engineering the response of these $BiFeO_3$-based systems for high-precision sensor or actuator devices where stability with driving fields and temperature are essential, will have to take into consideration the possible role of conductive DWs.

This work demonstrates that the local conductivity at DWs may have a dynamic role in ferroelectrics and may, thus, influence their macroscopic properties far more than so far considered.

4. Experimental Section

Sample Preparation and Characterization: According to the procedure described in ref. [42], "CG" $BiFeO_3$ ceramics were prepared by a two-step annealing procedure at 820 and 840 °C, whereas "FG" ceramics were prepared by sintering at 760 °C with a preceding annealing step at 600 °C. The final relative geometrical densities of all the samples were 93%. The average grain sizes, determined from SEM images of chemically etched samples, were 1.8 μm ± 0.9 μm and 16.0 μm ± 8.5 μm for the "FG" and "CG" samples, respectively. All the samples contained a minor concentration of secondary, non-perovskite phases, at the limit of X-ray diffraction (XRD) detection (Panalytical X'Pert Pro diffractometer with $K\alpha_1$ radiation). According to XRD analysis, the samples consist of randomly oriented grains. $Pb(Zr_{0.53}Ti_{0.47})O_3$ doped with 1 mol% Nb_2O_5 ("soft" PZT) and 0.5 mol% Fe_2O_3 ("hard" PZT), and $Pb(Zr_{0.75}Ti_{0.25})O_3$ ("undoped" PZT) were prepared by a conventional mixed-oxide route, as described in ref. [43]. The relative density and grain size of "soft," "hard," and undoped PZT samples were, respectively, 96% and 2.0 μm ± 0.8 μm, 98% and 2.2 μm ± 1.0 μm, and 96% and 8.5 μm ± 3.2 μm.

Piezoelectric and Dielectric Measurements: Electrical and electromechanical characterizations of $BiFeO_3$ and PZT samples were carried out on cylindrical samples thinned by SiC grinding paper to ≈0.5 mm and electroded with Au/Cr by sputtering. Samples were poled at room temperature using a DC field of 50 kV cm^{-1} ("FG" $BiFeO_3$) or 80 kV cm^{-1} ("CG" $BiFeO_3$), applied for 15 min. PZT samples were poled at room temperature by applying 30 kV cm^{-1} of DC field for 15 min. Converse piezoelectric measurements were performed using a fiber-optic displacement sensor (MTI 2100 Fotonic Sensor), a voltage generator (SRS DS360), a voltage amplifier (Trek 609E-6), an oscilloscope (LeCroy 9310C), and a lock-in amplifier (SR830 DSP). A cantilever was used as the upper mechanical contact, as reported in ref. [44]. The measurements were carried out at room temperature by using a continuous bipolar sinusoidal electric field of selected frequency and amplitude. The d_{33} was calculated as l_0/V_0, where l_0 and V_0 are the amplitudes of the displacement and voltage, respectively, and δ is the phase angle between the displacement and voltage signals. In the case of $BiFeO_3$, the values of d_{33} (≈30–70 pm V^{-1}) and δ could be measured with an accuracy of ±1.5 pm V^{-1} and ±0.3°, respectively, whereas those of PZT (d_{33} ≈ 450–540 pm V^{-1}) could be measured with an accuracy of ±10 pm V^{-1} and ±0.15°, respectively. These maximum deviations, from which the error bars were determined, were mostly related to the sample and cantilever positioning. Dielectric permittivity was determined using the same setup as described above for d_{33}, additionally equipped with a charge amplifier (Kistler 5018A), and under the same experimental conditions as used for the d_{33} measurements. The representation of the results for ε_{33} is the same as described above for d_{33}. The maximum variations in the measured values for ε_{33} and dielectric δ were related to charge drifts at low driving frequencies (<1 Hz). The error bars, shown on the graphs in Supporting Information Figure S1, were determined by performing several measurements, from which we evaluated the maximum relative variation in ε_{33} around a mean value.

AFM/PFM and SEM/EBSD Analyses: Surfaces of $BiFeO_3$ and PZT ceramic samples for AFM/PFM and SEM/EBSD analyses were prepared by standard metallographic procedures. After cutting, grinding with SiC, and polishing with a diamond paste, the sintered samples were etched by polishing for ≈20 min using a suspension consisting of 60 mL of OP-S silica colloidal suspension (Struers), 0.3 g of dissolved potassium hydroxide, and 440 mL of deionized water. For EBSD analysis, the samples were polished for a prolonged time, i.e., 2 h. Sample thicknesses ranged between 0.1 and 0.4 mm. Domain structure and phase composition of the samples were analyzed using a field-emission SEM (JSM-7600F) equipped with an energy-dispersive X-ray spectroscopy (EDXS) detector and EBSD analyzer (Oxford Instruments). The SEM/EDXS and EBSD analyses were performed using an acceleration voltage of 15 and 20 kV, respectively. PFM and *c*-AFM images were acquired using an AFM (Asylum Research, Molecular Force Probe 3D). A tetrahedral Si tip on a Si cantilever, both coated with Ti/Ir (Asyelec, AtomicForce F&E GmbH), was used. OP PFM images were acquired using a PFM Dual AC Resonance Tracking Switching Spectroscopy mode. Vector PFM mode was used to acquire OP and in-plane PFM images shown in the Supporting Information Figure S6. In both cases, we used 20 V of AC voltage on the tip. The PFM amplitude and phase signals from the analyzed samples were cross-checked by imaging a standard $LiNbO_3$ sample (Asylum Research, Periodically Poled Lithium Niobate Test Sample, AR-PPLN).[45] *c*-AFM experiments were conducted by applying a DC voltage between the tip and a bottom electrode. In selected sample regions, *c*-AFM imaging was done after the PFM imaging, where the later was used to identify the ferroelectric domains and DWs. The DC voltages used for *c*-AFM imaging were between ≈+10 and ≈+90 V and are specified in respective figure captions. The *c*-AFM images were acquired with a typical scan frequency and scan points/lines of 0.75 Hz and 400, respectively. Current profiles across selected lines on the samples' surfaces were measured using a lower scan frequency (0.1 Hz). Local *I*–*V* measurements were performed using a constant voltage rate of 1 V s^{-1}. A background current of ≈60 pA, detected at the limit of zero voltage (see, e.g., Figure 4c), was found to be mainly related to a voltage offset in the analog-to-digital converters in the controller unit.

Supporting Information

Supporting Information is available from the Wiley Online Library or from the author.

Acknowledgements

This work was financed by the Slovenian Research Agency (programme P2-0105 and project J2-5483). The work of D.D. was supported by the Swiss National Science Foundation (PNR62 Project No. 406240-126091). Centre of Excellence NAMASTE is acknowledged for access to the AFM/PFM equipment. David Žehelj, Maja Makarovič, Andraž Bradeško, Tomaž Kos, Bostjan Jančar, and Mihaela Rojac are acknowledged for their contributions.

Received: August 27, 2014
Revised: January 9, 2015
Published online: February 3, 2015

[1] N. Reyren, S. Thiel, A. D. Caviglia, L. Fitting Kourkoutis, G. Hammerl, C. Richter, C. W. Schneider, T. Kopp, A.-S. Rüetschi, D. Jaccard, M. Gabay, D. A. Muller, J.-M. Triscone, J. Mannhart, *Science* **2007**, *317*, 1196.

[2] N. D. Mathur, G. Burnell, S. P. Isaac, T. J. Jackson, B.-S. Teo, J. L. McManus-Driscoll, L. F. Cohen, J. E. Evetts, M. G. Blamire, *Nature* **1997**, *387*, 266.

[3] J. Seidel, L. W. Martin, Q. He, Q. Zhan, Y.-H. Chu, A. Rother, M. E. Hawkridge, P. Maksymovych, P. Yu, M. Gajek, N. Balke,

S. V. Kalinin, S. Gemming, F. Wang, G. Catalan, J. F. Scott, N. A. Spaldin, J. Orenstein, R. Ramesh, *Nat. Mater.* **2009**, *8*, 229.
[4] S. Farokhipoor, B. Noheda, *Phys. Rev. Lett.* **2011**, *107*, 127601.
[5] P. Maksymovych, J. Seidel, Y. H. Chu, P. Wu, A. P. Baddorf, L.-Q. Chen, S. V. Kalinin, R. Ramesh, *Nano Lett.* **2011**, *11*, 1906.
[6] Y. -P. Chiu, Y.-T. Chen, B.-C. Huang, M.-C. Shih, J.-C. Yang, Q. He, C.-W. Liang, J. Seidel, Y.-C. Chen, R. Ramesh, Y.-H. Chu, *Adv. Mater.* **2011**, *23*, 1530.
[7] R. J. Zeches, M. D. Rossell, J. X. Zhang, A. J. Hatt, Q. He, C.-H. Yang, A. Kumar, C. H. Wang, A. Melville, C. Adamo, G. Sheng, Y.-H. Chu, J. F. Ihlefeld, R. Erni, C. Ederer, V. Gopalan, L. Q. Chen, D. G. Schlom, N. A. Spaldin, L. W. Martin, R. Ramesh, *Science* **2009**, *326*, 977.
[8] J. Guyonnet, I. Gaponenko, S. Gariglio, P. Paruch, *Adv. Mater.* **2011**, *23*, 5377.
[9] P. Maksymovych, A. N. Morozovska, P. Yu, E. A. Eliseev, Y.-H. Chu, R. Ramesh, A. P. Baddorf, S. V. Kalinin, *Nano Lett.* **2012**, *12*, 209.
[10] M. Schröder, A. Haußmann, A. Thiessen, E. Soergel, T. Woike, L. M. Eng, *Adv. Funct. Mater.* **2012**, *22*, 3936.
[11] D. Meier, J. Seidel, A. Cano, K. Delaney, Y. Kumagai, M. Mostovoy, N. A. Spaldin, R. Ramesh, M. Fiebig, *Nat. Mater.* **2012**, *11*, 284.
[12] T. Sluka, A. K. Tagantsev, P. Bednyakov, N. Setter, *Nat. Commun.* **2013**, *4*, 1808.
[13] H. Béa, P. Paruch, *Nat. Mater.* **2009**, *8*, 168.
[14] G. Catalan, J. Seidel, R. Ramesh, J. F. Scott, *Rev. Mod. Phys.* **2012**, *84*, 119.
[15] E. I. Bondarenko, V. Y. Topolov, A. V. Turik, *Ferroelectr. Lett.* **1991**, *13*, 13.
[16] G. Arlt, N. A. Pertsev, *J. Appl. Phys.* **1991**, *70*, 2283.
[17] S. Li, A. S. Bhalla, R. E. Newnham, L. E. Cross, *Mater. Lett.* **1993**, *17*, 21.
[18] B. Jaffe, W. R. Cook, H. Jaffe, *Piezoelectric Ceramics*, Academic Press, London, UK **1971**.
[19] T. Sluka, A. K. Tagantsev, D. Damjanovic, M. Gureev, N. Setter, *Nat. Commun.* **2012**, *3*, 748.
[20] V. Porokhonskyy, Li Jin, D. Damjanovic, *Appl. Phys. Lett.* **2009**, *94*, 212906.
[21] D. Damjanovic, *J. Appl. Phys.* **1997**, *82*, 1788.
[22] V. Mueller, Y. Shchur, H. Beige, A. Fuith, S. Stepanow, *Europhys. Lett.* **2002**, *57*, 107.
[23] S. Li, W. Cao, L. E. Cross, *J. Appl. Phys.* **1991**, *69*, 7219.
[24] V. Mueller, Q. M. Zhang, *Appl. Phys. Lett.* **1998**, *72*, 2692.
[25] R. E. Eitel, T. R. Shrout, C. A. Randall, *J. Appl. Phys.* **2006**, *99*, 124110.
[26] D. Damjanovic, M. Demartin Maeder, P. Duran Martin, C. Voisard, N. Setter, *J. Appl. Phys.* **2001**, *90*, 5708.
[27] T. Rojac, A. Bencan, G. Drazic, M. Kosec, D. Damjanovic, *J. Appl. Phys.* **2012**, *112*, 064114.
[28] D. C. Sinclair, T. B. Adams, F. D. Morrison, A. R. West, *Appl. Phys. Lett.* **2002**, *80*, 2153.
[29] T. Furukawa, K. Ishida, E. Fukada, *J. Appl. Phys.* **1979**, *50*, 4904.
[30] H. Ueda, E. Fukada, F. E. Karasz, *J. Appl. Phys.* **1986**, *60*, 2672.
[31] A. V. Turik, G. S. Radchenko, *J. Phys. D* **2002**, *35*, 1188.
[32] A. V. Turik, A. I. Chernobabov, G. S. Radchenko, S. A. Turik, *Phys. Solid State* **2004**, *46*, 2213.
[33] V. V. Shvartsman, W. Kleemann, R. Haumont, J. Kreisel, *Appl. Phys. Lett.* **2007**, *90*, 172115.
[34] S. Farokhipoor, B. Noheda, *APL Mater.* **2014**, *2*, 056102.
[35] G. H. Jonker, *Solid-State Electron.* **1964**, *7*, 895.
[36] I. Stolichnov, M. Iwanowska, E. Colla, B. Ziegler, I. Gaponenko, P. Paruch, M. Huijben, G. Rijnders, N. Setter, *Appl. Phys. Lett.* **2014**, *104*, 132902.
[37] M. Valant, A. K. Axelsson, N. Alford, *Chem. Mater.* **2007**, *19*, 5431.
[38] Z. Li, H. Wu, W. Cao, *J. Appl. Phys.* **2012**, *111*, 024106.
[39] T. P. Comyn, T. Stevenson, A. J. Bell, *J. Phys. IV France* **2005**, *128*, 13.
[40] S. O. Leontsev, R. E. Eitel, *J. Mater. Res.* **2011**, *26*, 9.
[41] K. Yazawa, S. Yasui, H. Morioka, T. Yamada, H. Uchida, A. Gruverman, H. Funakubo, *J. Ceram. Soc. Jpn.* **2010**, *118*, 659.
[42] T. Rojac, M. Kosec, B. Budic, N. Setter, D. Damjanovic, *J. Appl. Phys.* **2010**, *108*, 074104.
[43] A. Benčan, B. Malič, S. Drnovšek, J. Tellier, T. Rojac, J. Pavlič, M. Kosec, K. G. Webber, J. Rödel, D. Damjanovic, *J. Am. Ceram. Soc.* **2012**, *95*, 651.
[44] N. P. Vyshatko, P. M. Brioso, J. P. Cruz, P. M. Vilarinho, A. L. Kholkin, *Rev. Sci. Instrum.* **2005**, *76*, 085101.
[45] T. Jungk, Á. Hoffmann, E. Soergel, *Appl. Phys. Lett.* **2006**, *89*, 163507.